Reaction pathways in remote plasma nitridation of ultrathin SiO_2 films

Hiro Niimi
Department of Physics, North Carolina State University, Raleigh, North Carolina 27695-8202

Amit Khandelwal and H. Henry Lamb,[a),b)]
Department of Chemical Engineering, North Carolina State University, Raleigh, North Carolina 27695-7905

Gerald Lucovsky,[a),c)]
Department of Physics, Materials Science and Engineering, and Electrical and Computer Engineering, North Carolina State University, Raleigh, North Carolina 27695-8202

(Received 27 February 2001; accepted for publication 24 September 2001)

Low-temperature nitridation of 3 nm SiO_2 films using He/N_2 and N_2 remote radio frequency (rf) plasmas was investigated. On-line Auger electron spectroscopy and angle-resolved x-ray photoelectron spectroscopy (ARXPS) were employed to determine the concentration, spatial distribution, and local chemical bonding of nitrogen in the resultant films. Experiments were performed using a substrate temperature of 300 °C and 30 W rf power. Nitridation using an upstream He/N_2 remote plasma at 0.1 Torr incorporates nitrogen at the top surface of the SiO_2 film. In contrast, a lower concentration of nitrogen distributed throughout the film is obtained when the process pressure is increased to 0.3 Torr. ARXPS indicates a $N–Si_3$ local bonding configuration, irrespective of the spatial distribution of N atoms. Slightly more nitrogen is incorporated using a downstream He/N_2 plasma at each process pressure. By comparison, nitridation of SiO_2 films using a N_2 remote plasma at 0.1 Torr is very slow. Optical emission spectroscopy indicates that He dilution enhances the generation of $N_2^+(B\,^2\Sigma_u^+)$ species by altering the plasma electron energy distribution and by providing an additional kinetic pathway (Penning ionization). Changing the He/N_2 remote plasma configuration from upstream to downstream (at 0.1 and 0.3 Torr) also enhances $N_2^+(B\,^2\Sigma_u^+)$ generation. For upstream He/N_2 remote plasmas, the intensity of N_2 first positive emission from $N_2(B\,^3\Pi_g)$ states increases with pressure, whereas the N_2^+ first negative emission from $N_2^+(B\,^2\Sigma_u^+)$ states decreases. We infer from these observations that N_2^+ species are primarily responsible for top surface nitridation at 0.1 Torr, and that neutral species [$N_2(A\,^3\Sigma_u^+)$ metastables and N atoms] are associated with sub-surface nitrogen incorporation. © *2002 American Institute of Physics.*
[DOI: 10.1063/1.1419208]

I. INTRODUCTION

Surface-channel devices, i.e., *p*-channel metal–oxide–semiconductor field-effect-transistor (*p*-MOSFET) with boron-doped (p^+) polycrystalline silicon (poly-Si) gate electrodes, have been shown to have better device characteristics than buried-channel *p*-MOSFET with arsenic- or phosphorus-doped (n^+) poly-Si gate electrodes.[1–7] They have better subthreshold cutoff characteristics and better ability to suppress short-channel effects, such as resistance to threshold lowering. However, there are some trade-offs between surface and buried-channel devices; e.g., the effective hole mobility of the buried-channel devices has been shown to be approximately 20% higher than that of surface channel devices.[2] Nevertheless, as device dimensions shrink, it is necessary to adopt a dual-gate complementary MOS (CMOS) structure, i.e., n^+ poly-Si gate electrode for *n*-channel MOS (NMOS) and p^+ poly-Si gate electrode for *p*-channel MOS (PMOS) devices, so that both devices are of the surface channel mode with proper short-channel characteristics.[7] This symmetric CMOS structure can scale to the minimum dimensions and reduce the operating voltage.

The boron-doped p^+ poly-Si gate-electrode for the PMOS device improves the short-channel effects; however, boron diffusion from the poly-Si gate-electrode into the channel region through the gate dielectrics can degrade PMOS device performance.[8–10] Therefore, for boron-doped p^+ poly-Si gate-electrode applications, it is necessary to have a diffusion barrier in the gate oxide to prevent the boron penetration into the Si substrate and the channel region.

Nitrogen atoms incorporated into the gate dielectric structure are one of candidates for blocking boron diffusion. Fair[11,12] predicted that less than 10 at. % of nitrogen in the oxide will have a negligible effect on boron diffusion. Therefore, to prevent boron diffusion from the p^+ poly-Si gate-electrode to the Si substrate requires a higher nitrogen concentration; e.g., at least 15–20 at. % at the $Si–SiO_2$ interface. However, ''light'' (monolayer-level) interfacial nitridation optimizes device performance and reliability.[13,14] This presents a dilemma. To block the boron at the $Si–SiO_2$ interface, one needs ''heavy'' nitridation. However, heavy interfacial nitridation degrades many aspects of device performance and reliability. Additionally, even if boron diffusion is prevented

[a)]Authors to whom correspondence should be addressed.
[b)]Electronic mail: lamb@eos.ncsu.edu
[c)]Electronic mail: gerry_lucovsky@ncsu.edu

by heavy nitridation at the $Si-SiO_2$ interface, boron can accumulate in the bulk oxide, and this accumulated boron in the oxide causes reliability degradation under gate injection; e.g., charge-to-breakdown and electron trapping.[15]

It is therefore important to suppress boron penetration at the ''top'' surface of the oxide, since a boron-blocking barrier on top of the oxide will prevent boron diffusion into the bulk oxide *and* to the $Si-SiO_2$ interface. The heavy nitridation layer can be far from the $Si-SiO_2$ interface. A heavy nitridation layer on the top surface of the oxide is not expected to reduce the device performance and reliability, and it has been shown that a top surface nitridation is an effective barrier to boron diffusion.[16]

There are two ways we can achieve this top surface nitridation: (i) by a nitridation of the top surface of a thin gate oxide and (ii) by a deposition of a thin Si_3N_4 film onto the gate oxide, as in a stacked O–N structure. Using remote plasma processing techniques, we can do both types of processing. We have previously reported top surface plasma nitridation of thermally grown oxides.[17] In addition, Hattangady *et al.*[18] have developed and applied this top plasma nitridation technology for CMOS device applications. Wu *et al.*[19] demonstrated an excellent PMOS device performance and reliability using plasma deposited Si_3N_4 film on the thermally grown oxide.

In this work, we investigated chemical reaction pathways for nitrogen incorporation at the top surface and in the ''bulk'' of 3-nm SiO_2 films. Nitridation was achieved (i) by using an upstream He/N_2 remote radio-frequency plasma in which both N_2 and He flow through the excitation zone and (ii) by injecting N_2 downstream of a He remote rf discharge, thus allowing only He atoms to be directly excited by plasma electrons. Nitridation experiments were performed at pressures of 0.1 and 0.3 Torr to elucidate the effects of pressure on the active nitrogen species in the remote plasma, and on the nitrogen concentrations and spatial distributions in the films. Nitridation at 0.1 Torr using an N_2 remote plasma (without He dilution) was examined for comparison. The resultant oxynitride films were characterized using Auger electron spectroscopy (AES) and angle-resolved x-ray photoelectron spectroscopy (ARXPS). Optical emission spectroscopy (OES) was employed to gain insight into the remote plasma chemistry.

II. EXPERIMENT

A. Apparatus

The nitridation experiments were performed using a remote plasma processing chamber that has been described previously.[14] The chamber has three main parts: (i) rf plasma tube (quartz tube with copper coil for rf excitation), (ii) gas dispersal ring (for downstream gas injection without plasma excitation), and (iii) substrate heater stage. A hybrid turbomolecular pump is used for process pumping.

B. Methods

The substrates were 50 mm diameter phosphorous-doped *n*-type Si(100) with a resistivity of 5.0–10.0 Ω cm ($\sim 5 \times 10^{15}\,cm^{-3}$). After wet chemical cleaning, a 10 nm thick sacrificial oxide was grown in a conventional thermal oxidation furnace at 900 °C, followed by 900 °C N_2 anneal for 20 min to reduce sub-oxides at the $Si-SiO_2$ interface. The samples were then dipped in a dilute HF (1 wt. %) solution to completely remove the sacrificial oxide. Immediately following the HF dip, each sample was rinsed in deionized H_2O, blown dry with N_2, and loaded in the load-lock chamber of the cluster tool.

The 3 nm SiO_2 films were deposited by remote plasma-enhanced chemical vapor deposition (RPECVD) and subsequently annealed at 900 °C. He/O_2 remote plasma exposure was used for interface formation, and a He/O_2 remote plasma with downstream injection of 2% SiH_4 in He was employed for bulk oxide deposition. The process temperature, pressure, and rf power were 300 °C, 0.3 Torr, and 30 W, respectively. After RPECVD, the wafer was transferred into a rapid thermal annealing chamber under high vacuum and annealed at 900 °C for 30 s in a 0.3 Torr He ambient. Nitridation was then performed using a He/N_2 or N_2 remote plasma at 0.1 Torr or 0.3 Torr. The He and N_2 flow rates (160 and 60 sccm, respectively) were set by mass flow controllers. Research grade He and N_2 were used. Nitridation was performed at a substrate temperature of 300 °C and rf power of 30 W. Nitridation using a N_2 remote plasma was performed at 0.1 Torr using a N_2 flow rate of 60 sccm.

C. Analysis

On-line AES using a 3 keV electron beam was performed in the ultrahigh vacuum (UHV) surface analysis chamber. AE spectra were collected in $N(E)$ mode using a single-pass cylindrical mirror analyzer and differentiated numerically. $dN(E)/dE$ spectra were used to quantify the nitrogen concentration at the top surface of the oxide using elemental sensitivity factors generated from Si, SiO_2 and Si_3N_4 standards. The following equation was used to estimate the atomic percent nitrogen [N]:

$$[\mathrm{N}] = \frac{\dfrac{I_\mathrm{N}}{S_\mathrm{N}}}{\dfrac{I_\mathrm{Si}}{S_\mathrm{Si}} + \dfrac{I_\mathrm{N}}{S_\mathrm{N}} + \dfrac{I_\mathrm{O}}{S_\mathrm{O}}} \times 100, \tag{1}$$

where I_N, I_Si, and I_O are the Auger intensities of N, Si, and O, respectively, and S_N, S_Si, and S_O are the relative sensitivities of N, Si, and O, respectively.[20]

ARXP spectra were measured *ex situ* using a PHI 3057 spectrometer comprising a 10–360 spherical capacitor analyzer, Omni Focus III fixed-aperture lens, 16-element multichannel detector, and 257 DR11 PC interface card. The Mg anode of a PHI 1248 dual-anode (Mg/Al) x-ray source was used. The XPS binding energies are referenced to the C 1*s* peak at 284.8 eV.

OES was used to characterize the remote rf plasmas. The plasma emission was sampled through a sapphire window (located 19 mm below the end of plasma tube and 13 mm above the gas dispersal ring) and transmitted via optical fiber to an EG&G Princeton Applied Research Model 1235 triple-grating spectrograph and optical multi-channel analyzer. A

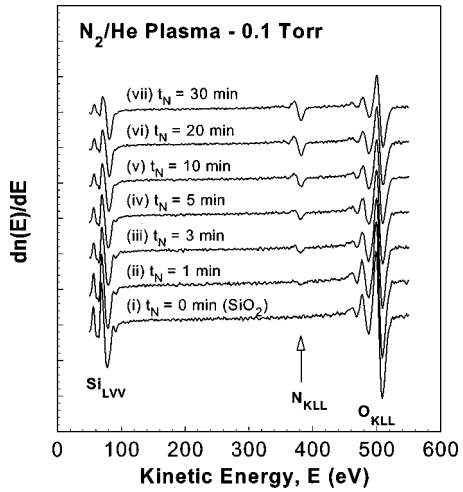

FIG. 1. AE spectra of a 3 nm SiO_2 film nitrided for different times at 0.1 Torr (upstream) and 30 W in He/N_2 plasma.

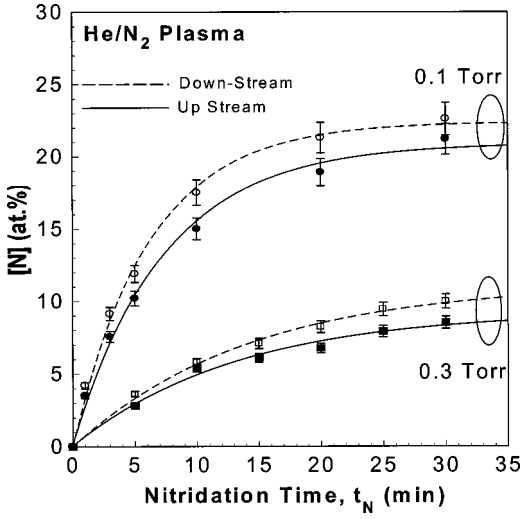

FIG. 3. Comparison of nitrogen concentration in a 3 nm SiO_2 film nitrided for different times at 0.1 and 0.3 Torr (upstream and downstream) and 30 W in He/N_2 plasma.

diffraction grating with 150 lines/mm, blazed at 650 nm, was used to record spectra between 350 and 950 nm.

III. RESULTS

A. On-line AES

1. Upstream He/N_2 *Process (I)*

Nitridation of a 3 nm SiO_2 film by an upstream remote plasma process in which both gases, N_2 and He, are subjected to plasma excitation was monitored by on-line AES. Figure 1 shows the AE spectra of (i) the bulk oxide deposition followed by the 900 °C anneal ($t_{ox}\sim 3.0$ nm) and (ii)–(vii) the film after exposure to the upstream He/N_2 remote plasma at 0.1 Torr from 1 to 30 min. As the He/N_2 plasma exposure time is increased, the N_{KLL} Auger peak at ~379 eV increases, and the Si_{LVV} feature (Si–O, at ~76 eV) and O_{KLL} feature at ~510 eV decrease. This shows that a longer He/N_2 plasma exposure time results in increased nitrogen incorporation in the SiO_2 film. Figure 2 shows the AE spectra of a 3 nm SiO_2 film exposed to an upstream He/N_2 remote plasma at a process pressure of 0.3 Torr for different exposure times. The nitrogen concentration increases with the plasma exposure time, but the concentration is always significantly less than for nitridation at 0.1 Torr.

Figure 3 compares the N concentration measured by AES for different nitridation times at 0.1 and 0.3 Torr. At both pressures, the N concentration initially increases with exposure time and then tends to saturate. The results indicate that increasing the process pressure from 0.1 to 0.3 Torr decreases the N concentration markedly. The nitridation rate (slope of [N] versus time plot in Fig. 3) is also higher at 0.1 Torr. The data fit the following pseudo-first-order kinetics expressions for upstream nitridation, as follows:

$$0.1\text{Torr} \qquad [\text{N}] = 20.4\{1-\exp(-0.14t_{\text{N}})\} \qquad (\text{at.}\,\%), \quad (2)$$

$$0.3\text{Torr} \qquad [\text{N}] = 9.25\{1-\exp(-0.075t_{\text{N}})\} \qquad (\text{at.}\,\%), \quad (3)$$

where t_{N} is the nitridation time in seconds. A comparison of Eqs. (2) and (3) indicates that decreasing the pressure from 0.3 to 0.1 Torr increases the nitridation rate and the amount of nitrogen incorporated in the SiO_2 films. The saturation N concentration at 0.3 Torr is less than half that of the 0.1 Torr process.

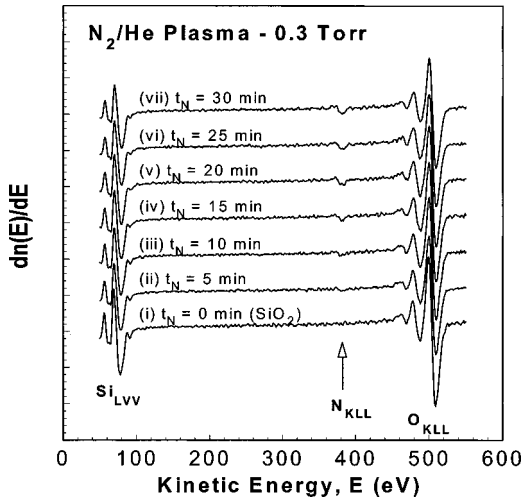

FIG. 2. AE spectra of a 3 nm SiO_2 film nitrided for different times at 0.3 Torr (upstream) and 30 W in He/N_2 plasma.

2. Downstream He/N_2 *process (II)*

In process II, N_2 is introduced through a gas dispersal ring downstream of the plasma tube, and He is passed through the plasma generation zone. Figure 3 includes a comparison of N concentration versus time for downstream and upstream He/N_2 remote plasma processes at 0.1 and 0.3 Torr. At each pressure, the saturation N concentration is greater for the downstream process than the upstream process. Greater N incorporation in the SiO_2 films takes place at 0.1 Torr than at 0.3 Torr, irrespective of reactor configuration.

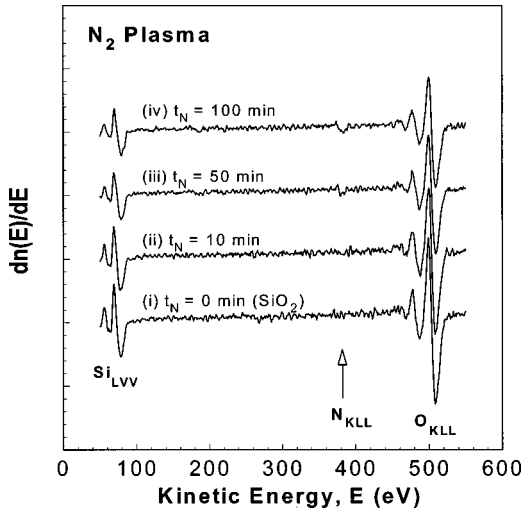

FIG. 4. AE spectra at different nitridation times for a 3 nm SiO_2 film nitrided by N_2 plasma (60 sccm) at 0.1 Torr and 30 W.

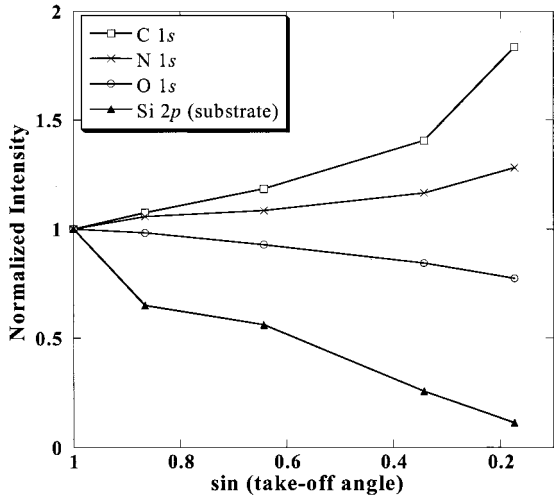

FIG. 6. Normalized N 1*s*, O 1*s*, Si 2*p*(substrate), and C 1*s* photoelectron signals as a function of sample orientation. The 3 nm SiO_2 film was nitrided for 30 min at 0.1 Torr (upstream) and 30 W in He/N_2 plasma.

3. N_2 *plasma process (III)*

A N_2 remote plasma (60 sccm) at 0.1 Torr was also used to nitride a 3 nm thick SiO_2 film. Figure 4 shows the AE spectra of the film after different N_2 plasma exposure times. It is evident that N_2 plasma nitridation is very slow compared to the He/N_2 plasma processes. The amount of nitrogen incorporated after 100 min using a N_2 remote plasma is significantly less than that incorporated after 30 min using a He/N_2 remote plasma at 0.1 Torr.

B. Angle-resolved XPS

Figure 5 shows the N 1*s* ARXP spectra of a 3 nm SiO_2 film nitrided using an upstream He/N_2 remote plasma at 30 W and 0.1 Torr for 30 min. XP spectra were taken at takeoff angles of 90°, 60°, 40°, 20°, and 10°. The takeoff angle is the angle between the wafer surface and the analyzer axis (see Fig. 5); at a takeoff angle of 90° the sample is normal to the analyzer axis. As the takeoff angle and hence the sampling depth are decreased, there is an increase in the N 1*s* peak intensity. Since the sampling volume is approximately constant, decreasing the takeoff angle enhances the signal from the top surface and vice-versa. Thus, the observed increase in the N 1*s* signal with decreasing takeoff angle evidences that nitrogen is located near the top surface. A distinct N 1*s* peak with a binding energy of 398.0 ± 0.1 eV is evident at each takeoff angle. The N 1*s* binding energy indicates $N–Si_3$ bonding in a SiO_xN_y matrix (see Sec. IV). The normalized N 1*s*, O 1*s*, Si 2*p*(substrate), and C 1*s* signals are shown in Fig. 6 as a function of the sine of the takeoff angle. The signals are normalized with respect to the Si 2*p*(oxide) signal, and each signal is self-normalized to 90° takeoff angle. Both the N 1*s* and C 1*s* signals increase with the decreasing takeoff angle, while the Si 2*p*(substrate) signal diminishes. The similar trends of the N 1*s* and C 1*s* peaks with takeoff angle indicate a similar spatial distribution. Since carbon is a surface contaminant, we conclude that for films nitrided at 0.1 Torr, nitrogen occupies the uppermost layer(s) of the film. ARXPS was also performed on a 3 nm SiO_2 film nitrided using a He/N_2 remote plasma at 30 W and 0.1 Torr for 3 min. A similar nitrogen spatial distribution and chemical bonding structure; i.e., N at the top surface bonded as $N–Si_3$, are indicated. However, the N concentration is comparable to that in films nitrided at 0.3 Torr for 30 min, consistent with the AES data (Fig. 3).

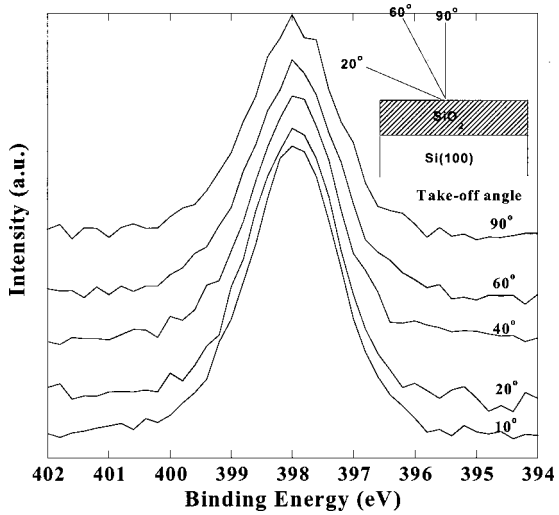

FIG. 5. N 1*s* photoelectron spectra for selected takeoff angles. The 3 nm SiO_2 film was nitrided for 30 min at 0.1 Torr (upstream) and 30 W in He/N_2 plasma.

Figure 7 shows the N 1*s* ARXP spectra of a 3 nm SiO_2 film nitrided using an upstream He/N_2 remote plasma at 0.3 Torr for 30 min. As the takeoff angle is decreased, the N 1*s* peak intensity diminishes. Since decreasing the takeoff angle enhances the surface sensitivity, this establishes that the nitrogen atoms are not at the top surface of the film, but are within the film or at the $Si–SiO_2$ interface. The measured N 1*s* binding energy of 398.3 ± 0.2 eV suggests $N–Si_3$ bonding in an SiO_xN_y matrix. Figure 8 shows the normalized N 1*s*, O 1*s*, Si 2*p*(substrate), and C 1*s* signals as a function of the sine of the takeoff angle. The N 1*s* and the O 1*s* signals

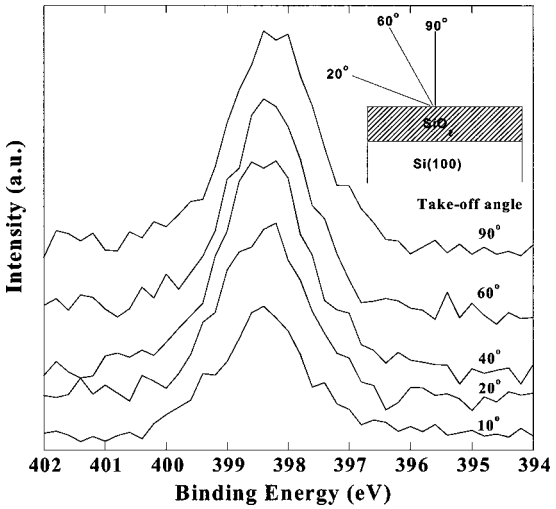

FIG. 7. N 1*s* photoelectron spectra for selected takeoff angles from a 3 nm SiO_2 film nitrided by He/N_2 plasma (at 0.3 Torr, upstream) for 30 min at 30 W.

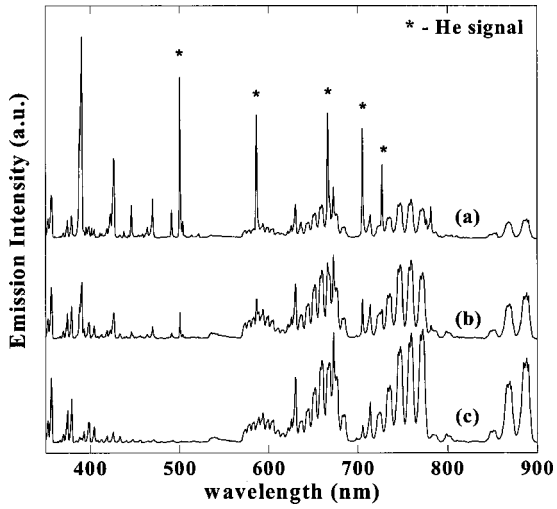

FIG. 9. Optical emission spectra of remote He/N_2 and N_2 plasmas at 0.1 Torr and applied power: 30 W (a) He(160 sccm)/N_2(60 sccm) plasma (downstream) (b) He(160 sccm)/N_2(60 sccm) plasma (upstream), and (c) undiluted N_2 (60 sccm) plasma (upstream).

follow similar trends with decreasing takeoff angle. This indicates that N is present throughout the film and is not associated preferentially with the $Si–SiO_2$ interface. Nitridation at 0.3 Torr in the downstream configuration gives a similar result. The N 1*s* intensity decreases with takeoff angle, and the normalized N 1*s* and O 1*s* signals track each other as the XPS sampling depth is changed. We conclude that He/N_2 remote plasma nitridation at 0.3 Torr, irrespective of the process configuration (upstream or downstream), results in N incorporation throughout the film.

C. Optical emission spectroscopy

OES was used to detect electronically excited atomic and molecular species in the He/N_2 and N_2 remote plasmas in both the upstream and downstream configurations. Figure 9 compares the OE spectra of He(160 sccm)/N_2(60 sccm) plasmas (upstream and downstream) with a N_2 plasma (60 sccm). The pressure and applied power were 0.1 Torr and 30 W, respectively. In addition to numerous He emission lines (at 388, 500, 586, 667, 706 and 727 nm), peaks associated with the N_2 first positive (denoted "1+") and second positive (denoted "2+") series and the N_2^+ first negative series (denoted "1−") are observed. The N_2 1+ series, which arises from $B\,^3\Pi_g \rightarrow A\,^3\Sigma_u^+$ transitions, appears as five broad bands of regularly spaced peaks in the visible and near infrared spectral regions. The strongest 1+ peaks of each band occur at emission wavelengths of 541, 594, 661, 773 and 889 nm. The strongest peaks of the 2+ series, which involves $C\,^3\Pi_u \rightarrow B\,^3\Pi_g$ transitions, occur at 296, 315, 337, 358, 380, 400 and 427 nm. Intense peaks of the 1− series of N_2^+ molecular ion transitions ($B\,^2\Sigma_u^+ \rightarrow X\,^2\Sigma_g^+$) are observed at 391.4 and 426.4 nm for He/N_2 plasmas. Emission from excited nitrogen atoms at 821.6 nm is not detectable. Other atomic nitrogen peaks completely overlap the strong N_2 1+ series peaks. The N_2^+ 1− emission lines are stronger for the He/N_2 plasmas than the N_2 plasma, and in the downstream configuration as compared to the upstream configuration. The He emission lines are also stronger for the downstream configuration. The N_2 1+ emission is more intense for the N_2 plasma than the He/N_2 plasmas. The N_2 1+ intensity decreases when the source is operated in the downstream configuration.

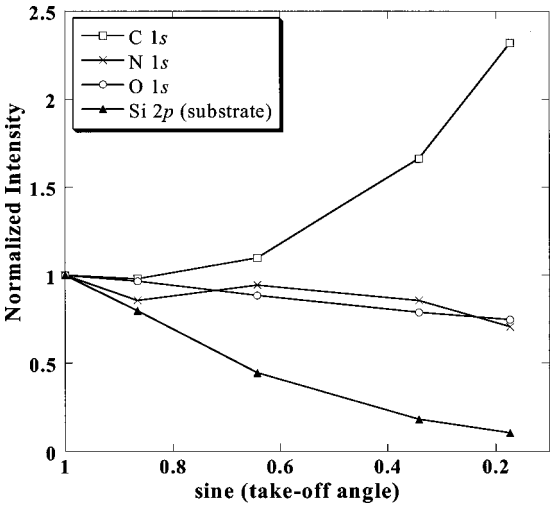

FIG. 8. Normalized N 1*s*, O 1*s*, Si 2*p*(substrate), and C 1*s* photoelectron signals as a function of sample orientation. The 3 nm SiO_2 film was nitrided for 30 min at 0.3 Torr (upstream) and 30 W in He/N_2 plasma.

Figure 10 compares the OE spectra of He/N_2 remote plasmas (upstream and downstream) and a N_2 remote plasma (180 sccm) at 0.3 Torr. The N_2^+ 1− intensities are greater for He/N_2 plasmas than for the N_2 plasma. The N_2^+ 1− and He emission intensities increase when N_2 is introduced downstream through a gas dispersal ring. The N_2 1+ emission intensity is slightly greater for the upstream configuration as compared to the downstream configuration. The N_2 1+ intensity at 889 nm for the He/N_2 plasma in the upstream configuration is comparable to that of the N_2 plasma at 0.3 Torr; however, 1+ emission in the visible range and 2+ emission is significantly more intense for the He/N_2 plasma.

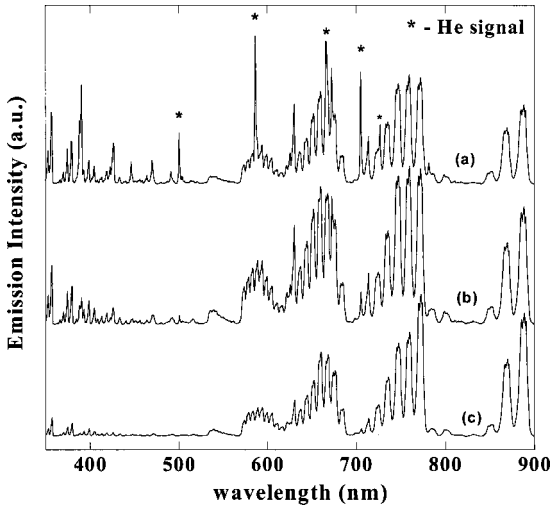

FIG. 10. Optical emission spectra of remote He/N_2 and N_2 plasmas at 0.3 Torr and applied power: 30 W (a) He(160 sccm)/N_2(60 sccm) plasma (downstream) (b) He(160 sccm)/N_2(60 sccm) plasma (upstream), and (c) undiluted N_2 (180 sccm) plasma (upstream).

Figure 11 shows the effect of pressure on the He (500 nm), N_2^+ 1− (391 nm) and N_2 1+ (889 nm) emission intensities for an upstream He/N_2 remote plasma. The N_2 1+ intensity at 889 nm increases significantly with pressure. Conversely, increasing the process pressure decreases the intensities of N_2^+ 1− and He emission lines.

IV. DISCUSSION

The nitrogen concentration distributions resulting from He/N_2 remote plasma exposure of 3 nm SiO_2 films at 0.1 and 0.3 Torr are illustrated schematically in Fig. 12. At 0.1 Torr, the nitrogen is confined to a ~1 nm layer near the top surface. Secondary ion mass spectroscopy measurements indicate that the nitrogen concentration in the surface layer is approximately $5\times10^{22}\,cm^{-3}$.[21] When the process pressure is increased to 0.3 Torr, the nitridation rate decreases markedly,

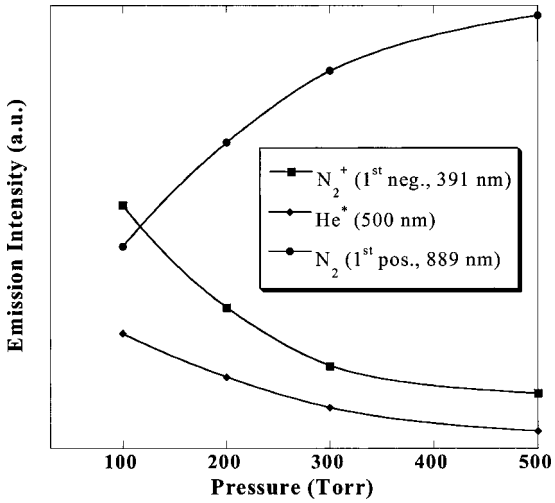

FIG. 11. Intensities of N_2^+ (391 nm), He (500 nm), and N_2 1+(889 nm) optical emission lines as a function of pressure for the for He/N_2 remote plasmas (upstream).

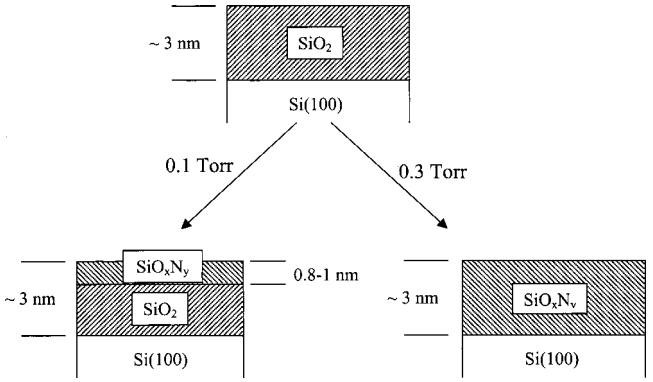

FIG. 12. Schematic representation of the nitridation process and the resultant N distribution for a He/N_2 plasma at (a) 0.1 Torr and (b) 0.3 Torr

and a relatively uniform nitrogen concentration is obtained throughout the ~3 nm film. For ultrathin SiO_2 films (<1 nm) processed at 0.3 Torr, previous experiments have shown that nitrogen diffuses through the superficial oxide, and bonds at the $Si–SiO_2$ interface.[21,22] These observations suggest that the nitridation mechanism changes from ''nondiffusive'' (charged particle-assisted) to ''diffusive'' (presumably involving neutral N species) as the process pressure is increased from 0.1 to 0.3 Torr. The very low nitridation rate measured at 0.1 Torr using a N_2 remote plasma indicates that He dilution provides a strong nitridation rate enhancement.

The N 1*s* binding energies determined by ARXPS evidence that the local chemical environment of nitrogen in the oxynitride films is closely similar to that in Si_3N_4. N 1*s* binding energies between 397.4 and 397.7 eV have been reported for the $N–Si_3$ bonding configuration in silicon nitride (Si_3N_4).[23–25] Since oxygen is more electronegative than nitrogen, replacement of N second nearest neighbors by O leads to a small positive binding energy shift. The binding energy shift will depend on the number of N atoms replaced by more electronegative O atoms, and hence there will be a range of N 1*s* binding energies.[26] Thus, the small difference between the N 1*s* binding energies for top surface nitridation at 0.1 Torr (398.0±0.2 eV) and for sub-surface nitridation at 0.3 Torr (398.3±0.2 eV) is attributed to the nitrogen concentration difference. [$(Si–)_2N–O$] and related structures with a N–O bond are ruled out since there is no evidence of a N 1*s* peak at ~400 eV.[25]

The OE spectra of the N_2 and He/N_2 remote plasmas may be interpreted using a simplified set of elementary reactions.[27] Collisions of plasma electrons with ground-state nitrogen molecules result in excitation and ionization:

$$N_2(X\,^1\Sigma_g^+)+e^-\rightarrow N_2(C\,^3\Pi_u)+e^-, \tag{4}$$

$$N_2(X\,^1\Sigma_g^+)+e^-\rightarrow N_2^+(X\,^2\Sigma_g^+)+2e^-. \tag{5}$$

The electron energies required for these reactions are ~11 and ~16 eV, respectively, and they occur primarily within the plasma generation region where the electron density is highest. The excited N_2 species cascade rapidly to the $N_2(A)$ metastable state via 2+ and 1+ emission:

$$N_2(C\,^3\Pi_u)\rightarrow N_2(B\,^3\Pi_g)+h\nu(2+), \tag{6}$$

$$N_2(B\,^3\Pi_g) \rightarrow N_2(A\,^3\Sigma_u^+) + h\nu(1+). \quad (7)$$

The $N_2(C)$, $N_2(B)$, $N_2(A)$ triplet states have radiative lifetimes of 40 ns, ~6 μs, and ~2 s, respectively.[28] Thus, the strong 2+ and 1+ emission bands observed from the He/N_2 and N_2 remote plasmas indicate the presence of N_2 triplet excited states, and the band intensities are a good measure of the $N_2(A)$ generation rate via radiative cascade. Vibrationally excited $N_2(C)$ species ($v>4$) also undergo predissociation:[27]

$$N_2(C)(v>4) \rightarrow N(^4S) + N(^2D). \quad (8)$$

Consequently, the He/N_2 and N_2 remote plasmas may contain chemically significant concentrations of N atoms. Unfortunately, neither of these atomic N species can be detected directly by OES since the $^2D \rightarrow {}^4S$ radiative transition is forbidden by dipole selection rules. The $N_2(B)$ initial state of the 1+ series, however, is also produced via recombination of ground-state $N(^4S)$ atoms.[29,30]

The N_2^+ 1− emission intensities are proportional to the $N_2^+(B)$ concentrations in the remote plasmas. The $N_2^+(B)$ state can be generated by direct electron impact ionization of ground-state N_2 (requiring a threshold energy of 18.7 eV), electron excitation of ground-state $N_2^+(X)$, and Penning ionization involving He metastables. The $N_2^+(B)$ concentrations in N_2 remote plasmas at 0.1 and 0.3 Torr are quite small, as evidenced by the very weak N_2^+ 1− emission intensities. The addition of He (160 sccm) to N_2 (60 sccm) remote plasmas at 0.1 and 0.3 Torr significantly enhances the N_2^+ 1− emission intensity. Emission from excited He atoms is observed, but the He emission lines are significantly less intense than for a He remote plasma with downstream N_2 addition [compare Figs. 9(a) and 9(b)]. The He emission intensity is a good measure of the production rate of He metastables [$2\,^3S$(19.82 eV) and $2\,^1S$(20.6 eV)] via radiative cascade and direct excitation.[31] Due to its higher ionization potential (24.6 eV), the addition of He to a N_2 remote plasma alters the electron energy distribution (EED), increasing the high-energy electron population. The observed emission from He excited states with energies of ~23 eV above the ground state supports this conclusion. Thus, in a He/N_2 remote plasma there is a higher density of electrons with sufficient energy to produce the $N_2^+(B)$ state by ionization of ground-state N_2:

$$N_2(X\,^1\Sigma_g^+) + e^- \rightarrow N_2^+(B\,^2\Sigma_u^+) + 2e^-. \quad (9)$$

In addition, the $N_2^+(B)$ state can be formed via Penning ionization:

$$He(2\,^3S) + N_2(X\,^1\Sigma_g^+) \rightarrow N_2^+(B\,^2\Sigma_u^+) + e^- + He. \quad (10)$$

Since this reaction has a large cross section,[32] it may provide a significant additional pathway to $N_2^+(B)$ generation. We infer from these observations that He/N_2 remote plasmas are likely to contain higher concentrations of N_2^+ species than N_2 remote plasmas when operated under similar conditions.

The effects of He dilution on the generation of N_2 triplet excited states are more subtle. The addition of He to a N_2 remote plasma at 0.1 Torr decreases the N_2 1+ and 2+ emission intensities, and the vibrational state distributions of the excited N_2 molecules do not change significantly. These observations are consistent with a simple dilution effect. He addition at 0.3 Torr, however, results in an increase in the integrated intensity of the 1+ and 2+ emission bands and alters the vibrational state distributions of the excited N_2 molecules. These observations cannot be explained by excitation transfer from He metastables due to the large energy mismatch with the $N_2(C)$ state. The N_2 triplet excited states are more efficiently generated by energy transfer from electrons and by energy pooling reactions involving N_2 metastables.[33] The OE spectra are indicative of a higher concentration of $N_2(A)$ metastables in a He/N_2 remote plasma at 0.3 Torr than in a N_2 remote plasma operated under similar conditions.

The OES results also suggest that increasing the process pressure increases the $N_2(A)$-to-N_2^+ ratio in the He/N_2 remote plasmas. The He and N_2^+ 1− emission intensities decrease, and the N_2 1+ emission intensity increases with increasing pressure (Fig. 11). Increasing the process pressure reduces the mean free path and favors recombination and de-excitation reactions. Consequently, at higher pressures the plasma afterglow does not extend as far into the downstream region. A secondary effect of increasing process pressure is to alter the plasma EED via energy transfer from electrons to neutrals (thermalization), thereby reducing the average electron temperature and suppressing the high-energy tail of the EED. Fewer electrons are available with sufficient energy to populate the high-lying electronically excited states of He and to generate the $N_2^+(B)$ state by ionization of ground-state N_2. Conversely, electronic excitation of N_2 molecules is favored by a higher neutral density and lower electron temperature, and this results in greater emission from N_2 triplet states at higher pressures. Thus, the OE spectra of remote He/N_2 plasmas are consistent with a trend of increasing the $N_2(A)$-to-N_2^+ ratio with increasing pressure. The most marked change occurs between 0.1 and 0.3 Torr, as illustrated by the OE intensity data in Fig. 11.

In the downstream configuration, He atoms are excited within the plasma generation region, and the resulting He metastables, He^+ ions, and electrons interact with N_2 molecules that are injected downstream. The strong He emission lines evidence the generation of He metastables, and the intense N_2^+ 1− emission indicates the generation of $N_2^+(B)$ species. The N_2^+ 1− emission is more intense when a He/N_2 remote plasma is operated in the downstream configuration, irrespective of process pressure. We infer that higher concentrations of He metastables and high-energy electrons are available downstream of a He remote plasma, thereby increasing the rate of $N_2^+(B)$ generation via Eqs. (9) and (10). Conversely, changing the reactor configuration from upstream to downstream decreases the N_2 1+ and 2+ emission intensities, since the $N_2(C)$ state is generated primarily by direct electron excitation in the plasma generation region [Eq. (4)],

V. CONCLUSIONS

Top surface nitridation of 3 nm SiO_2 films is readily achieved using a 30 W He/N_2 remote plasma at 0.1 Torr. By

comparison, nitridation using a N_2 remote plasma at 0.1 Torr is very slow, demonstrating that He dilution provides a significant rate enhancement. We infer from OE spectra that a He/N_2 remote plasma is rich in N_2^+ species and deficient in $N_2(A)$ metastables relative to a N_2 remote plasma, when both are operated at 0.1 Torr and 30 W. He dilution alters the plasma EED by increasing the high-energy electron population and provides an additional pathway to N_2^+ generation via Penning ionization. These observations lead us to conclude that N_2^+ species are primarily responsible for top surface nitridation. When the process pressure is increased to 0.3 Torr, the nitridation rate decreases markedly, and a uniform nitrogen concentration is obtained throughout the 3 mm film. At 0.3 Torr, the plasma afterglow does not extend as far into the downstream region, and the $N_2(A)$-to-N_2^+ ratio in the remote He/N_2 plasma is increased. Thus, we conclude that neutral nitrogen species [$N_2(A)$ metastables and N atoms] are primarily responsible for SiO_2 nitridation using a He/N_2 remote plasma at 0.3 Torr. Slightly higher nitrogen concentrations are obtained in SiO_2 films by using downstream He/N_2 remote plasmas, irrespective of process pressure.

ACKNOWLEDGMENTS

This work is funded in part by the Office of Naval Research, the SEMATECH/Semiconductor Research Corporation Front End Processes Center, and the Air Force Office of Scientific Research.

[1] J. Y.-C. Sun, Y. Taur, R. H. Dennard, S. P. Klepner, and L. K. Wang, Tech. Dig. - Int. Electron Devices Meet. **1986**, 236.
[2] G. J. Hu and R. H. Bruce, IEEE Trans. Electron Devices **ED-32**, 584 (1985).
[3] S. J. Hillenius, R. Liu, G. E. Georgiou, R. L. Field, D. S. Williams, A. Kornblit, D. M. Boulin, R. L. Johnston, and W. T. Lynch, Tech. Dig. - Int. Electron Devices Meet. **1986**, 252.
[4] N. Kasai, N. Endo, and H. Kitajima, Tech. Dig. - Int. Electron Devices Meet. **1987**, 367.
[5] K. Tanaka and M. Fukuma, Tech. Dig. - Int. Electron Devices Meet. **1987**, 328.
[6] B. Davari *et al.* Tech. Dig. - Int. Electron Devices Meet. **1988**, 56.
[7] C. Y. Wong, J. Y.-C. Sun, Y. Taur, C. S. Oh, R. Angelucci, and B. Davari, Tech. Dig. - Int. Electron Devices Meet. , 238 (1988).
[8] J. Y.-C. Sun, C. Wong, Y. Taur, and C.-H. Hsu, 1989 Symposium VLSI Technical Digest, p. 17.
[9] J. R. Pfiester, F. K. Baker, T. C. Mele, H.-H. Tseng, P. J. Tobin, J. D. Hayden, J. W. Miller, G. C. D. Parrillo, and L. C. Parrillo, IEEE Trans. Electron Devices **ED-37**, 1842 (1990).
[10] K. S. Krisch, L. Manchanda, F. H. Baumann, M. L. Green, D. Brasen, F. L. C. and A. Ourmazd, Tech. Dig. - Int. Electron Devices Meet. , 325 (1994).
[11] R. B. Fair, in The Physics and Chemistry of SiO_2 and the Si-SiO_2 Interface-3, edited by H. Z. Massoud, E. H. Poindexter, and C. R. Helms (The Electrochemical Society, Pennington, NJ, 1996), pp. 200–213.
[12] R. B. Fair, J. Electrochem. Soc. **144**, 708 (1997).
[13] H. S. Momose, T. Morimoto, Y. Ozawa, K. Yamabe, and H. Iwai, IEEE Trans. Electron Devices **41**, 546 (1994).
[14] H. Niimi and G. Lucovsky, J. Vac. Sci. Technol. A **17**, 3185 (1999).
[15] D. Wrister, L. K. Han, T. Chen, H. H. Wang, D.-L. Kowng, M. Allen, and J. Fulford, Appl. Phys. Lett. **68**, 2094 (1996).
[16] K. A. Ellis and R. A. Buhrman, J. Electrochem. Soc. **145**, 2068 (1998).
[17] S. V. Hattangady, H. Niimi, and G. Lucovsky, Appl. Phys. Lett. **66**, 3495 (1995).
[18] S. V. Hattangady, R. Kraft, D. T. Drider, M. A. Douglas, G. A. Brown, P. A. Tiner, J. W. Kuehne, P. E. Nicollian, and M. F. Pas, Tech. Dig. - Int. Electron Devices Meet. **1996**, 495.
[19] Y. Wu, G. Lucovsky, and H. Z. Massoud, Proceedings of the IEEE International Reliability Physics Symposium, 1998, p. 70.
[20] L. E. Davis, N. C. MacDonald, P. W. Palmberg, G. E. Riach, and R. E. Weber, *Handbook of Auger Electron Spectroscopy: A Reference Book of Standard Data for Identification and Interpretation of Auger Electron Spectroscopy Data* (Physical Electronics Industries, Inc., Eden Prairie, MN 1987).
[21] H. Niimi and G. Lucovsky, J. Vac. Sci. Technol. B **17**, 2610 (1999).
[22] A. Khandelwal, B. C. Smith, and H. H. Lamb, J. Appl. Phys. **90**, 3100 (2001).
[23] M. Bhat, G. W. Yoon, J. Kim, D. L. Kwong, M. Arendt, and J. M. White, Appl. Phys. Lett. **64**, 2116 (1994).
[24] J. L. Bischoff, F. Lutz, D. Bolmont, and L. Kubler, Surf. Sci. **251/252**, 170 (1991).
[25] S. R. Kaluri and D. W. Hess, J. Electrochem. Soc. **144**, 2200 (1997).
[26] S. I. Raider, R. Flitsch, J. A. Aboat, and W. A. Pliskin, J. Electrochem. Soc. **123**, 560 (1976).
[27] A. N. Wright and C. A. Winkler, *Active Nitrogen* (Academic, New York, 1968).
[28] R. D. Kenner and E. A. Ogryzlo, in *Chemi- and Bioluminescence*, edited by J. G. Burr (Marcel Dekker, New York, 1985).
[29] K. D. Bayes and G. B. Kistiakowsky, J. Chem. Phys. **32**, 992 (1960).
[30] J. Berkowitz, W. A. Chupka, and G. B. Kistiakowsky, J. Chem. Phys. **25**, 457 (1956).
[31] D. V. Tsu, G. N. Parsons, and G. Lucovsky, J. Vac. Sci. Technol. A **6**, 1849 (1988).
[32] M. Cher and C. S. Hollingsworth, J. Chem. Phys. **50**, 4942 (1969).
[33] L. G. Piper, J. Chem. Phys. **91**, 864 (1989).